INFLUENCE OF EARTH'S SHADOWING EFFECTS ON SPACE DEBRIS STABILITY

C. Hubaux

Namur Center for Complex Systems (NAXYS), University of Namur
Rempart de la Vierge 8, B-5000 Namur, Belgium
Email: charles.hubaux@unamur.be

ABSTRACT

In this work, we present results about the stability of near-geosynchronous space debris characterized by high area-to-mass ratios. We extend previous studies by considering the influence of the Earth's shadow on the short- and long-term time evolutions. To assess the orbits stability, we use the Global Symplectic Integrator (GSI) [18] which consists in the symplectic integration of both Hamiltonian equations of motion and variational equations. The solution of the variational equations is then used to compute the Mean Exponential Growth factor of Nearby Orbits (MEGNO) chaos indicator. The effects of the Earth's shadow are analyzed using the adapted conical and cylindrical Earth's shadowing models introduced by [10]. Our stability study shows that the Earth's shadow greatly affects the global behaviour of space debris orbits by increasing the size of chaotic regions around the geostationary altitude.

Key words: Geostationary orbit ; stability ; solar radiation pressure ; Earth's shadow.

1. INTRODUCTION

Understanding the behaviour of space debris orbits is a matter of great importance. The stability of near-geosynchronous space debris characterized by high area-to-mass ratios is investigated. Different meanings are usually associated to the term *stability*. In our case, unstable orbits correspond to *unpredictable* orbits, i.e. orbits which are very sensitive to initial conditions.

Around the geostationary altitude, orbital periods are close to one sidereal day, leading to a 1:1 resonance with the Earth's rotational period. A previous study [3] already showed that chaotic orbits are present very close to the separatrices of this resonant structure, due to irregular transits between the libration and circulation regimes. Perturbations taken into account were the geopotential up to degree and order two, luni-solar gravitational attraction and direct solar radiation pressure. Then, the same region has been studied [26] with increased values of the area-to-mass ratio, showing that the higher this ratio, the less predictable the orbits around the separatrices. A complex structure of secondary resonances was also identified [16] inside the resonance.

In this work, we extend previous studies by considering the influence of the Earth's shadow on the short- and long-term time evolutions of space debris. To assess the orbits stability, we use the Mean Exponential Growth factor of Nearby Orbits (MEGNO), which is an efficient numerical tool to distinguish between regular and chaotic behaviors. To reliably compute long-term space debris motion, we resort to the Global Symplectic Integrator (GSI) [18] which enables the simultaneous symplectic integration of both Hamiltonian equations of motion and variational equations. The solution of the variational equations is then used to compute the MEGNO. The effects of the Earth's shadow are analyzed using the adapted conical and cylindrical Earth's shadowing models introduced by [10]. The smooth shadow function deriving from these models can be easily included into the variational equations and was proven to deliver accurate shadow models on very long periods of time. Our stability study shows how the resonance eye is affected by the presence of the Earth's shadow on long time scales. We also emphasize the differences in the results given by conical or cylindrical Earth's shadowing. Full details are available in [11].

First, the model used to reproduce space debris orbital perturbations is presented in Sec. 2. Then we briefly describe the method and the tools needed for the stability study in Sec. 3. The results are shown in Sec. 4 and we conclude in Sec. 5.

2. MODEL

The long period of time (300 yr) targeted for this study makes very suitable the use of symplectic integrators. Indeed, such schemes present excellent energy preservation properties and are often less time-consuming than non-symplectic schemes due to larger time steps. In this study we consider the Earth's gravitational attraction, luni-solar gravitational perturbations and solar radiation pressure.

Proc. '6th European Conference on Space Debris'
Darmstadt, Germany, 22–25 April 2013 (ESA SP-723, August 2013)

The corresponding Hamiltonian can be written as

$$\begin{aligned}\mathcal{H}(\vec{v},\Lambda,\vec{r},\theta) &= \frac{v^2}{2} + \dot{\theta}\Lambda \\ - &\quad \frac{\mu}{R_\oplus}\sum_{n=0}^{\infty}\sum_{m=0}^{n}(C_{nm}V_{nm}(\mathbf{r},\theta)+S_{nm}W_{nm}(\mathbf{r},\theta)) \\ - &\quad \sum_i \mu_i\left(\frac{1}{\|\vec{r}-\vec{r}_i\|}-\frac{\vec{r}\cdot\vec{r}_i}{\|\vec{r}_i\|^3}\right) \\ - &\quad C_r\frac{1}{\|\vec{r}-\vec{r}_\odot\|}P_r\frac{A}{M}a_\odot^2 \end{aligned} \quad (1)$$

where $\vec{r} := (x, y, z)$ and $\vec{v}$ are respectively the Cartesian geocentric coordinates and velocities of the satellite in the fixed inertial equatorial geocentric frame, $r := \|\vec{r}\|$ and $v := \|\vec{v}\|$ are their norms, θ is the Greenwich sidereal time, Λ is its associated momentum and $\mu = \mathcal{G}M_\oplus$ is the standard gravitational coefficient.

The angular derivative $\dot{\theta}$ is assumed constant in the part accounting for the rotation of the Earth around its axis of smallest inertia.

The complete Earth's potential is expressed in the frame rotating around the Earth's axis of smallest inertia and with the same angular speed. The equatorial Earth's radius is denoted $R_\oplus$ and C_{nm} and S_{nm} are the spherical harmonics coefficients (see e.g. [13]). The recursive functions V_{nm} and W_{nm} are described in [6] and later in [22] and let us write the geopotential with Cartesian coordinates. The Earth's gravity model is the *EGM96* one described in [17].

As many third bodies as wanted could be taken into account. In this work, we mainly consider the Sun and the Moon. The geocentric Cartesian coordinates of any third body of mass M_i are denoted $\vec{r}_i$ and $\mu_i = \mathcal{G}M_i$. For the purpose of this stability analysis the positions and velocities are evaluated by means of a subroutine created by P. Exertier (OCA Grasse)[1].

The force induced by the solar radiation pressure is obtained by adding together the elementary forces accounting for the absorption, reflection and diffusion effects. The model assumes a spherical shape for debris and no radiation from the surface of the Earth. Detailed information about the model can be found in [21]. The parameters are C_r a dimension-free reflectivity coefficient fixed to one in this work, $\vec{r}_\odot$ the geocentric Cartesian position of the Sun, $P_r = 4.56 \times 10^{-6}\, N/m^2$ the radiation pressure for an object located at a distance of 1 AU from the Sun, A/M the area-to-mass ratio of debris and $a_\odot$ the mean distance between the Sun and the Earth (i.e. $a_\odot = 1$ AU). Due to some assumptions, the solar radiation pressure contribution is written under its conservative form.

Cylindrical Earth's shadow crossings are modeled by multiplying the gradient of the radiation pressure part of the Hamiltonian in equations of motion by a smooth shadow function equal to one when debris are in direct sunlight and zero otherwise (see [10]). This function is defined as

$$\nu_{\mathrm{c}}(\vec{r}) := \frac{1}{2}\Big\{1+\tanh[\gamma\, s_{\mathrm{c}}(\vec{r})]\Big\} \quad (2)$$

where the auxiliary function

$$s_{\mathrm{c}}(\vec{r}) := \frac{\vec{r}\cdot\vec{r}_\odot}{r_\odot} + \sqrt{r^2 - R_\oplus^2}$$

is smaller than zero when debris are in Earth's umbra (inspired from [9]) and γ is a precision parameter set to 10^9 to represent cylindrical shadow crossings. Using this method forces us to reduce the integration time step. The latter must be small enough to perform some steps inside the umbra zone, which only represents a small part of the total revolution time. On a geostationary orbit, a typical shadow crossing only lasts around half an hour. Let us note though that it makes possible the use of low order symplectic integrators, still keeping accurate results. This smooth formulation is particularly suitable for symplectic integrators but can be used for any other kind of propagator.

Going one step further, umbra-penumbra transitions can be modeled by adapting the previous formulae. As presented with full details in [10], the constant γ must be modified to change the shape of the shadow function. Analytical developments yield

$$\nu_{\mathrm{p}}(\vec{r}) = \frac{1}{2}\left\{1+\tanh\left[\frac{\delta 2\pi R_\oplus}{\Delta h(\vec{r})}s_{\mathrm{c}}(\vec{r})\right]\right\} \quad (3)$$

where

$$\begin{aligned}\Delta h(\vec{r}) \;=\; & \cos\alpha\left[\sqrt{r^2 - R_\oplus^2\cos^2\alpha} + R_\oplus\sin\alpha\right] \\ & -\cos\beta\left[\sqrt{r^2 - R_\oplus^2\cos^2\beta} - R_\oplus\sin\beta\right]\end{aligned}$$

with

$$\alpha = \operatorname{atan}\frac{R_\odot - R_\oplus}{\|\vec{r}-\vec{r}_\odot\|} \quad \text{and} \quad \beta = \operatorname{atan}\frac{R_\odot + R_\oplus}{\|\vec{r}-\vec{r}_\odot\|}.$$

Angles α and β give the difference between the umbra cylinder and respectively the umbra and penumbra cones, and $R_\odot$ denotes the Sun radius. The ν_{p} shadow function is smooth, equal to one in direct sunlight, starts to decrease in the penumbra cone and is equal to zero in the umbra cone. The parameter δ is another accuracy parameter set to 8 in the forthcoming simulations. As explained in [11], small variations of this parameter have been tested, leading to the same conclusions in the stability study.

3. METHOD

The GSI method has been described in [18] and analyzed further in [11].

[1] This model is based on Brown's theory of the mean motion of both Moon and Sun [20].

It has been successfully validated on the well-known Hénon-Heiles Hamiltonian and restricted three-body problem in [18]. In this case, the SALI chaos indicator [25] was used along with the symplectic schemes from [14].

In [11] the MEGNO has been used, based on the important advantage that it only needs the time evolution of a single deviation vector (the SALI requires the evolution of two deviation vectors to be known). It is especially convenient for space debris stability issues where integrations act on long time spans and involve a lot of initial conditions. This combination of the GSI with the MEGNO has successfully been checked on the Arnold diffusion phenomenon occuring along the resonances of the Hamiltonian model described in [15]. It has also been noted that the integrators defined in [27] should be preferred to the ones from [14] in the framework of the GSI.

In this section we briefly present the GSI method, the symplectic integrator that will be used and the MEGNO.

3.1. GSI

Let us consider an autonomous Hamiltonian system with N degrees of freedom $\mathcal{H}(\vec{p},\vec{q})$. Equations of motion can be written as

$$\dot{\vec{x}} = \mathcal{J}\vec{\nabla}_{\vec{x}}\mathcal{H} = W(\vec{x})\,, \tag{4}$$

where $\vec{x} = \begin{pmatrix} \vec{p} \\ \vec{q} \end{pmatrix} \in \mathbb{R}^{2N}$ and

$$\mathcal{J} = \begin{pmatrix} 0_N & -1_N \\ 1_N & 0_N \end{pmatrix} \tag{5}$$

is the standard symplectic matrix, 1_N is the $N \times N$ identity matrix and 0_N the $N \times N$ null matrix.

Chaos indicators like the MEGNO are based on the time evolution of deviation vectors which represent infinitesimal displacements from the orbit. These vectors, $\vec{\delta} = (\vec{\delta}_p, \vec{\delta}_q) \in \mathbb{R}^{2N}$, satisfy the variational equations given by

$$\dot{\vec{\delta}} = D_{\vec{x}}W\vec{\delta}(t) = \mathcal{J}\nabla^2_{\vec{x}}\mathcal{H}\,\vec{\delta} \tag{6}$$

where $D_{\vec{x}}W$ is the Jacobian matrix of the vector field W and $\nabla^2_{\vec{x}}\mathcal{H}$ is the Hessian matrix of $\mathcal{H}$. One easily proves that the vector field (6) is Hamiltonian and associated to the *variational* Hamiltonian given by

$$\mathcal{K}(\vec{x},\vec{\delta}) = \frac{1}{2}\vec{\delta}^T\nabla^2_{\vec{x}}\mathcal{H}(\vec{x})\vec{\delta}. \tag{7}$$

The GSI has been introduced in [18] to numerically integrate both systems of equations (4) and (6) in a symplectic way. The symplectic integrator that will be used assumes that $\mathcal{H}$ is split into two separately integrable parts, A and B. Besides we impose the condition that A and B respectively depend on $\vec{p}$ and $\vec{q}$:

$$\mathcal{H}(\vec{p},\vec{q}) = A(\vec{p}) + B(\vec{q}). \tag{8}$$

Easy calculation shows that the variational equations (6) can be written as

$$\begin{pmatrix} \dot{\vec{\delta}}_p \\ \dot{\vec{\delta}}_q \end{pmatrix} = \begin{pmatrix} -\vec{\nabla}_{\vec{\delta}_q}\mathcal{B} \\ \vec{\nabla}_{\vec{\delta}_p}\mathcal{A} \end{pmatrix} \tag{9}$$

and the variational Hamiltonian (7) becomes

$$\begin{aligned} \mathcal{K}(\vec{p},\vec{q},\vec{\delta}_p,\vec{\delta}_q) &= \frac{1}{2}\vec{\delta}_p^T\nabla^2_{\vec{p}}A\vec{\delta}_p + \frac{1}{2}\vec{\delta}_q^T\nabla^2_{\vec{q}}B\vec{\delta}_q \\ &= \mathcal{A}(\vec{p},\vec{\delta}_p) + \mathcal{B}(\vec{q},\vec{\delta}_q)\,. \end{aligned} \tag{10}$$

3.2. Integrator

The equations of motion (4) can be written as

$$\dot{\vec{x}} = L_{\mathcal{H}}\vec{x} = \{\mathcal{H},\vec{x}\} = \sum_{j=1}^{N}\frac{\partial\mathcal{H}}{\partial p_j}\frac{\partial\vec{x}}{\partial q_j} - \frac{\partial\mathcal{H}}{\partial q_j}\frac{\partial\vec{x}}{\partial p_j}.$$

The operator $L_{\mathcal{H}}\bullet$ is used as another notation for Poisson brackets $\{\mathcal{H},\bullet\}$.

The solution of this differential equation can be expressed as

$$\vec{x}(t) = e^{tL_{\mathcal{H}}}\vec{x}(t_0) = \sum_{j=0}^{\infty}\frac{t^j}{j!}L^j_{\mathcal{H}}\vec{x}(t_0) \tag{11}$$

where t_0 is the initial time and t is the time where $\vec{x}$ needs to be evaluated.

Considering the splitting of the Hamiltonian (8), the Campbell-Baker-Hausdorff formula is used in [27] to successively build second- and fourth-order integrators[2]

$$\begin{aligned} S_2(t) &= e^{\frac{t}{2}L_A}e^{tL_B}e^{\frac{t}{2}L_A} \\ S_4(t) &= S_2(\gamma_0 t)S_2(\gamma_1 t)S_2(\gamma_0 t) \end{aligned}$$

where

$$\gamma_0 = -\frac{2^{1/3}}{2-2^{1/3}} \quad \text{and} \quad \gamma_1 = -\frac{1}{2-2^{1/3}}.$$

Such schemes approximate $e^{tL_{\mathcal{H}}}$ and mean that we exactly evaluate $\mathcal{E}$ where

$$\mathcal{E} = \mathcal{H} + \mathcal{O}(t^{n+1})$$

where n is respectively equal to 2 and 4 for the second- and fourth-order integrators.

Conveniently, the same symplectic scheme can be used to integrate both systems (4) and (6). One easily shows that both $\mathcal{H}$ and $\mathcal{K}$ can be split into two parts, one of which depending only on momenta and the other one only on coordinates.

[2] Higher orders are also described in [27] but will not be used in this study.

3.3. MEGNO

According to [5], the MEGNO is defined as

$$Y(t) = \frac{2}{t}\int_0^t \frac{\dot{\delta}(s)}{\delta(s)} s\, ds \tag{12}$$

where $\delta = \|\vec{\delta}\|$. It is in fact very similar to the Lyapunov Characteristic Exponent (LCE) [2]. For a given orbit, the LCE is defined as

$$\sigma = \lim_{t\to\infty} \frac{1}{t} \ln \frac{\delta(t)}{\delta(0)}.$$

It measures the mean exponential rate of divergence of nearby orbits. It can also be expressed as

$$\sigma = \lim_{t\to\infty} \frac{1}{t}\int_0^t \frac{\dot{\delta}(s)}{\delta(s)} ds. \tag{13}$$

While both formulae (12) and (13) are close to each other the LCE computation is more time consuming.

A useful indicator is given by the time average of the MEGNO:

$$\overline{Y}(t) = \frac{1}{t}\int_0^t Y(s)\, ds. \tag{14}$$

While $Y(t)$ might neither converge nor admit a limit for $t \to \infty$, it has been proven by [5] that the asymptotic value of $\overline{Y}$ provides a good characterization of the regular or chaotic nature of orbits.

One advantage of the MEGNO with respect to the LCE is that it can be expressed as a sum, whatever the considered orbit. The asymptotic behaviour of $\overline{Y}(t)$ writes

$$\overline{Y}(t) \simeq ct + d$$

where $(c, d) \simeq (\sigma/2, 0)$ for irregular orbits. However, $(c, d) \simeq (0, 2)$ for stable quasi-periodic orbits, $d \lesssim 2$ for orbits close to periodic stable ones and $d \gtrsim 2$ for orbits closed to unstable periodic ones. Second, one can show that $\lim_{t\to\infty} Y/t = \sigma$ for chaotic orbits and that Y/t reaches 0 faster than the LCE does for regular orbits. Interested readers can find a detailed analytical description of the evolution of the MEGNO in [5] and a comparison between different chaos indicators in [19].

As explained in [11], a convenient approach to solve both integrals defining the MEGNO and its time average with the GSI is a simple but efficient trapezoidal rule. It yields

$$Y(t+\tau) = \frac{t}{t+\tau} Y(t) + \frac{2t+\tau}{t+\tau} \ln \frac{\delta(t+\tau)}{\delta(t)} + \mathcal{O}(\tau^3) \tag{15}$$

and

$$\overline{Y}(t+\tau) = \frac{1}{t+\tau}[t\overline{Y}(t) + 0.5\tau(Y(t) + Y(t+\tau))] + \mathcal{O}(\tau^3)\,. \tag{16}$$

MEGNO values represented in the results are in fact mean MEGNO values (16) computed at the end of the time interval.

4. RESULTS

The analysis has been performed on a grid (160×160) of initial osculating semi-major axes a and resonant angles σ_{res}. It lets us study the evolution of the 1:1 mean motion resonance appearing in this plane. The resonant angle σ_{res} is defined as $\lambda - \theta$ where λ and θ are respectively the initial mean longitude and sidereal time. Around the geostationary altitude, both angle frequencies are very close to each other.

First we show the stability results when the model includes the central body attraction, the geopotential up to degree and order 2, luni-solar perturbations and solar radiation pressure without Earth's shadow. As described in [26], the two-dimensional space (σ_{res}, a) is characterized by separatrices (already identified in [3]) and an additional pattern inside the *eye of the resonance*. Due to the important amount of CPU time needed, we only plot an horizontal range of 160 deg. Hence we only see one eye of the typical double pendulum-like pattern related to the 1:1 resonance. The large area-to-mass is responsible for the stochastic zones in the neighborhood of the separatrices. The pattern inside the resonance has been explained by secondary resonances due to commensurabilities between the resonant angle and the ecliptic longitude of the Sun [16]. Computing the MEGNO for such a huge number of initial conditions is excessively time consuming. Hence, propagations realized in [26] usually stopped at 30 yr. Here we push it further and compute the final values of the MEGNO with the GSI and S_4 integrator after 300 yr. As in the rest of the paper, small time steps equal to 0.01 day/2π have been used. The value of the initial sidereal time θ is determined by the initial time epoch at 25 January 1991 and the initial conditions are set to $e = 0.002$, $i = 0.004$ rad and $\Omega = \omega = 0$ rad. The area-to-mass ratio is equal to 5 m^2/kg. The map shown in Fig. 1 lets us emphasize the presence of stable orbits when there is no umbra even after 300 yr. The unstable separatrices are clearly visible.

Cylindrical shadow crossings are then added thanks to the shadow function (2). We show in Fig. 2 the (σ_{res}, a) plane for an integration time of 30 yr. The chaos map obtained with the cylinder-shaped umbra leads to unrealistic results. The entire map is filled with chaotic orbits, at the exception of very few stable orbits located on the separatrices.

Then, the long term stability of space debris subject to conical Earth's shadow crossings is investigated. We show in Fig. 3 the MEGNO values obtained after 300 yr with conical shadow. Nearly all orbits are identified as chaotic. A close look to data shows that only a very small amount of initial conditions lead to a final MEGNO value smaller than 2. Hence, the GSI tells us that the introduction of Earth's shadowing effects greatly influences the behaviour of space debris orbits. As time increases, chaotic areas around the separatrices grow and even the center of the resonance seems to become unstable.

Eventually, one could wonder if the same results hold

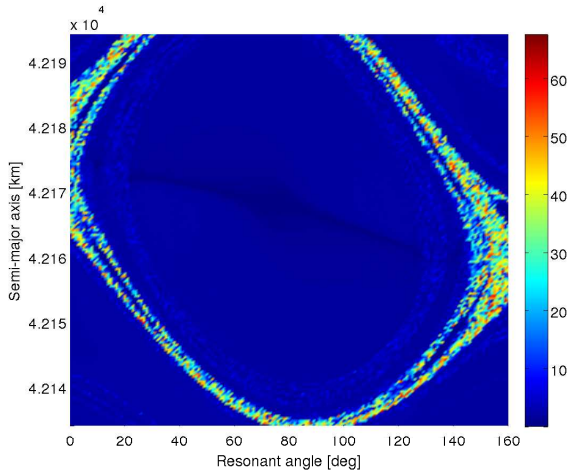

Figure 1. Stability analysis of the two-dimensional plane (σ_{res}, a) represented using MEGNO values at 300 yr without Earth's shadow crossings.

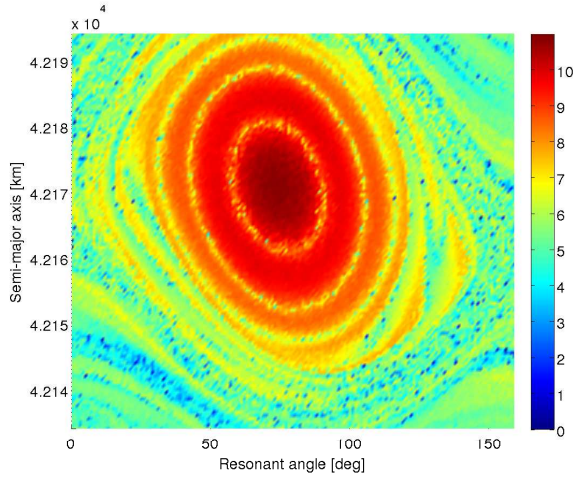

Figure 2. Stability analysis of the two-dimensional plane (σ_{res}, a) represented using MEGNO values at 30 yr with cylindrical Earth's shadow crossings.

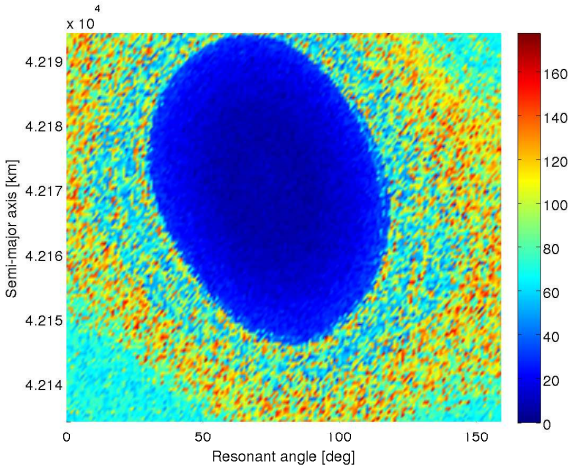

Figure 3. Stability analysis of the two-dimensional plane (σ_{res}, a) represented using MEGNO values at 300 yr with conical Earth's shadow crossings.

for space debris with much lower area-to-mass ratios. A comprehensive and systematic approach showing stability results for increasing values of the area-to-mass ratio over 300 yr is unrealistic in terms of CPU time. However, one can reasonably suppose that, the lower the area-to-mass ratio, the more regular space debris orbits. More insight about this assumption is brought by means of a stability map realized with the area-to-mass ratio set to 0.01 m^2/kg. The results are shown in Fig. 4 after 30 yr. The thick chaotic separatrix has given way to more constraint irregular motion. Both vertical lines appearing around $\sigma_{\rm res} \simeq 35$ deg and $\sigma_{\rm res} \simeq 40$ deg are due to missing data.

Other tests have been realized with a non-symplectic method. Even if the long time span means a potential important loss of accuracy, such comparisons are helpful. We resorted to the tenth-order Adams-Bashforth-Moulton integrator developed in NIMASTEP (see [8]). The results reveal that chaotic orbits also fill the entire plane (a few number of stable orbits in the vicinity of the stable equilibrium excepted). The global behaviour is in agreement with our previous study.

5. CONCLUSION

The GSI method with the MEGNO has been applied to produce two-dimensional stability maps of the near-geostationary altitude. Both cylindrical and conical shadow models have been tested. Both the GSI and the non-symplectic scheme highlighted the poor usability of the cylindrical model in this framework. However, the conical shadow model seems well handled by the GSI. Simulations with a high area-to-mass ratio (5 m^2/kg) let us see the strong influence of shadow crossings on space debris stability. Chaotic zones around the separatrices of the 1:1 resonance (already present without shadow) grow

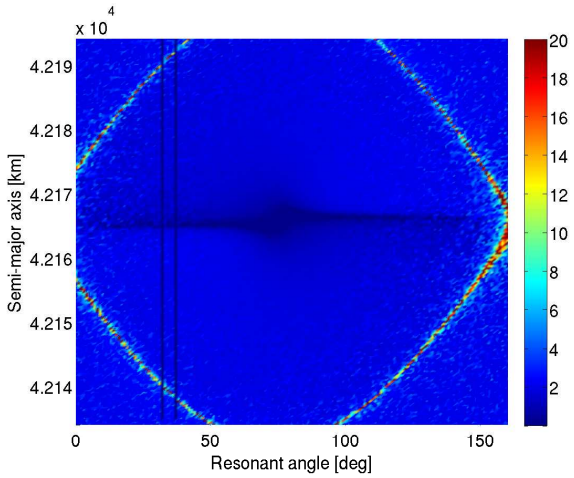

Figure 4. Stability analysis of the two-dimensional plane (σ_{res}, a) *represented using MEGNO values at* 30 *yr with conical Earth's shadow crossings and a small area-to-mass ratio (*0.01 *m^2/kg).*

and progressively fill the entire plane, destroying the resonant structure. It should be noted that the lower the area-to-mass ratio values (a simulation was performed with an area-to-mass ratio around 0.01 m^2/kg), the more regular the orbits in the plane. In this case, chaotic orbits are mainly confined around the thin separatrices.

Let us mention that our stability investigations about near-geostationary debris could be extended to other types of orbits. One could for example focus on Medium Earth Orbits on which GPS and GALILEO navigation satellites stay. While existing works on this topic have already been published (among which one can cite [4, 24, 23, 12, 1, 7]), stability studies like the one developed here could bring new perspectives.

ACKNOWLEDGMENTS

The work of Ch. Hubaux is supported by an FNRS Ph.D Fellowship. This research used resources of the Interuniversity Scientific Computing Facility located at the University of Namur, Belgium, which is supported by the F.R.S.-FNRS under convention No. 2.4617.07. This paper presents research results of the Belgian Network DYSCO (Dynamical Systems, Control, and Optimization), funded by the Interuniversity Attraction Poles Programme, initiated by the Belgian State, Science Policy Office. The scientific responsibility rests with its author(s).

REFERENCES

1. Anselmo, L. and Pardini, C. (2011). Orbital evolution of the first upper stages used for the new European and Chinese navigation satellite systems. *Acta Astronaut.*, **68**, 2066-2079

2. Benettin, G., Galgani, L., Giorgilli, A., and Strelcyn, J.-M. (1980). Lyapunov characteristic exponents for smooth dynamical systems and for Hamiltonian systems; a method for computing all of them, part 1: theory. *Meccanica*, **15**, 9-20

3. Breiter, S., Wytrzyszczak, I. and Melendo, B. (2005). Long-term predictability of orbits around the geosynchronous altitude. *Adv. Space Res.*, **35**, 1313-1317

4. Chao, C. C. and Gick, R. A. (2004). Long-term evolution of navigation satellite orbits: GPS/GLONASS/GLONASS. *Adv. Space Res.*, **34**, 1221-1226

5. Cincotta, P., Giordano, C., and Simó, C. (2003). Phase Space structure of multi-dimensional systems by means of the mean exponential growth factor of nearby orbits. *Physica D*, **182**, 151-178

6. Cunningham, L. E. (1970). On the computation of the spherical harmonic terms needed during the numerical integration of the orbital motion of an artifical satellite. *Celest. Mech. Dyn. Astr.*, **2**, 207-216

7. Deleflie, F., Rossi, A., Portmann, C., Métris, G., and Barlier, F. (2011). Semi-analytical investigations of the long term evolution of the eccentricity of Galileo and GPS-like orbits. *Adv. Space Res.*, **47**, 811-821

8. Delsate, N. and Compère, A. (2012). NIMASTEP: a software to modelize, study, and analyze the dynamics of various small objects orbiting specific bodies. *Astron. Astrophys.*, **540**

9. Escobal, P. (1976). *Methods of Orbit Determination*, Krieger, 2nd ed

10. Hubaux, C., Lemaître, A., Delsate, N. and Carletti, T. (2012). Symplectic integration of space debris motion considering several Earth's shadowing models. *Adv. Space Res.*, **49**, 1472-1486

11. Hubaux, C., Libert, A.-S., Delsate, N. and Carletti, T. (2013). Influence of Earth's shadowing effects on space debris stability. *Adv. Space Res.*, **51**, 25-38

12. Jenkin, A. B. and McVey, J. P. (2009). Constellation and "graveyard" collission risk for several MEO disposal strategies. In *Proceedings of the Fifth European Conference on Space Debris, ESA SP-672. ESA Publications Division., Noordwijk, The Netherlands.*

13. Kaula, W. M. (1966). *Theory of Satellite Geodesy: Applications of Satellites to Geodesy*, Blaisdell Publishing Company

14. Laskar, J. and Robutel, P. (2001). High order symplectic integrators for perturbed Hamiltonian systems. *Celest. Mech. Dyn. Astr.*, **80**, 39-62

15. Lega, E., Guzzo, M. and Froeschle, C. (2003). Detection of Arnold diffusion in Hamiltonian systems. *Physica D*, **182**, 179-187

16. Lemaître, A., Delsate, N., and Valk, S. (2009). A web of secondary resonances for large A/m geostationary debris. *Celest. Mech. Dyn. Astron.*, **104**, 383-402

17. Lemoine, F., Kenyon, S., Factor, J., and et al. (1987). The development of the joint NASA GSFC and NIMA geopotential model EGM96. *Technical report*, NASA, TP-1998-206861

18. Libert, A.-S., Hubaux, C. and Carletti, T. (2011). The Global Symplectic Integrator: an efficient tool for stability studies of dynamical systems. Application to the Kozai resonance in the restricted three-body problem. *Mon. Not. R. Astron. Soc.*, **414**, 659–667

19. Maffione, N. P., Darriba, L. A., Cincotta, P. M., and Giordano, C. M. (2013). Chaos detection tools: application to a self-consistent triaxial model. *Mon. Not. R. Astron. Soc.*, **429**, 2700-2717

20. Meeus, J. (1988). *Astronomical Formulae for Calculators*, Willmann-Bell Inc, 4th ed Enlarged and Revised

21. Milani, A. and Gronchi, G. (2009). *Theory of orbit determination*, Cambridge University Press, 1st ed

22. Montenbruck, O. and Gill, E. (2005). *Satellite Orbits*, Springer

23. Rossi, A. (2008). Resonant dynamics of Medium Earth Orbits: space debris issues. *Celest. Mech. Dyn. Astr.*, **100**, 267-286

24. Saunders, C. J., E., M. C., and Lewis, H. G. (2005). Disposal orbit characteristics for GALILEO including orbit propatation techniques. In *Danesy, D. (Ed), Proceedings of the Fourth European Conference on Space Debris, ESA SP-587. ESA Publications Division., Noordwijk, The Netherlands*, pp. 79-284

25. Skokos, C. (2001). Alignment indices: A new, simple method for determining the ordered or chaotic nature of orbits.*J. Phys. A*, **34**, 10029-10043

26. Valk, S., Delsate, N., Lemaitre, A. and Carletti, T. (2009). Global dynamics of high area-to-mass ratios GEO space debris by means of the MEGNO indicator. *Adv. Space Res.*, **43**, 1509-1526.

27. Yoshida, H. (1990). Construction of higher order symplectic integrators. *Phys. Lett. A*, **150**, 262-268